Dynamics of Atmospheres and Oceans 93 (2021) 101206

Contents lists available at ScienceDirect

Dynamics of Atmospheres and Oceans

journal homepage: www.elsevier.com/locate/dynatmoce

Resolution of the atmospheric model matters for the Northern Hemisphere Mid-Holocene climate

Gerrit Lohmann [a,b,*], Axel Wagner [a,b], Matthias Prange [b]

[a] Alfred-Wegener-Institut Helmholtz-Zentrum für Polar- und Meeresforschung, Bussestraße 24, 27570 Bremerhaven, Germany
[b] MARUM – Zentrum für Marine Umweltwissenschaften, Universität Bremen, Leobener Str. 8, 28359 Bremen, Germany

ARTICLE INFO

Keywords:
Paleoclimate modeling
Resolution
Mid-Holocene

ABSTRACT

This study evaluates the dependence of simulated surface air temperatures on model resolution and orography for the mid-Holocene. Sensitivity experiments with the atmospheric general circulation model ECHAM5 are performed with low (~3.75°, 19 vertical levels) and high (~1.1°, 31 vertical levels) resolution. Results are compared to the respective preindustrial runs. It is found that the large-scale temperature anomalies for the mid-Holocene (compared to preindustrial) are significantly different in the low- and high-resolution versions. For boreal winter, differences are mainly related to circulation changes caused by the response to thermal forcing in conjunction with orographic resolution. For summer, shortwave cloud radiative forcing emerges as an important factor. The anomaly differences (low minus high resolution version) in the Northern Hemisphere are regionally as large as the anomalous mid-Holocene temperature signals. Furthermore, they depend on the applied surface boundary conditions. We conclude that the resolution matters for the Northern Hemisphere response in mid-Holocene simulations, which should be taken into account in model-model and data-model comparisons.

1. Introduction

Modelling the Holocene climate has been a focus for the Paleoclimate Modelling Intercomparison Project (PMIP) since its beginning (Joussaume and Taylor, 1995), progressing from simulations with atmospheric general circulation models, using prescribed ocean conditions, to simulations using fully coupled atmosphere–ocean-sea ice general circulation models, some of which included vegetation dynamics (Kageyama et al., 2006; Braconnot et al., 2007a,b, 2012), to simulations with more full Earth system models (e.g., Otto-Bliesner et al., 2017). At the same time, the grid resolution has increased in these climate models from ~5° to now ~1° horizontal resolution with more accurate simulations of physical processes on a more local scale. One key aspect of the intercomparisons is to evaluate and benchmark models, assembling evaluation data sets and undertaking quantitative assessment of simulations. One particular source of uncertainty in climate models is due to their spatial resolution (Randall et al., 2007; Flato et al., 2013). Small-scale physical processes that cannot be resolved adequately on the computational mesh are represented as parameterized schemes. By improving computer architectures and resources, higher resolved models are applied. Model results of simulations with enhanced grid resolution demonstrate more realistic climate simulations, e.g. due to the growing set of model processes and phenomena (Roeckner et al., 2006; Bader et al., 2008; Reichler and Kim, 2008; Lauer and Hamilton, 2013; Lohmann et al., 2020).

* Corresponding author at: Alfred-Wegener-Institut Helmholtz-Zentrum für Polar- und Meeresforschung, Bussestraße 24, 27570 Bremerhaven, Germany.
E-mail address: gerrit.lohmann@awi.de (G. Lohmann).

https://doi.org/10.1016/j.dynatmoce.2021.101206
Received 3 April 2020; Received in revised form 13 November 2020; Accepted 24 January 2021
Available online 30 January 2021

The resolution in numerical simulations of the atmosphere is thus of particular interest. The orographic boundary condition, as an example, shows substantial differences between coarse and higher resolved model setups. As a response, the meridional vorticity gradient could lead to a modified atmospheric Rossby wave propagation (Charney and Eliassen, 1949; Bolin, 1950; Kasahara, 1966; Yoshino, 1981; Cook and Held, 1992), in response to sea surface temperature (SST) forcing (Houghton et al., 1974; Huang, 1978; Chervin et al., 1980; Hoskins and Karoly, 1981; Simmonds and Smith, 1986; Hoskins and Ambrizzi, 1993). Aside from orographic boundary conditions, the tuning of parameterized subgrid-scale processes is indispensable in climate models of varying grid size (Kiehl and Williamson, 1991; Kristjánsson, 1991; Lane et al., 2000; Tselioudis and Jakob, 2002; Jung and Arakawa, 2004).

Concerning model inter-comparison studies, experiments have been carried out with a wide spectrum of models involving different parameterization schemes, complexities and resolution (Cubasch et al., 2001; Braconnot et al., 2012; Knutti and Sedláček, 2012). As one particular example, Roeckner et al. (2006) performed a set of experiments with the atmospheric general circulation model ECHAM5 with prescribed SSTs (Roeckner et al., 2003). The resolutions ranged from T21L19 to T159L31. While the physics of the model remained unchanged, resolution-sensitive parameters were changed (Roeckner et al., 2006). The results show a tendency to reduce the error upon increasing horizontal and vertical resolution.

Regarding model inter-comparisons for the modern climate, Cess et al. (1990) focussed on global atmospheric feedback processes. The treatment of cloud processes was identified as responsible for intermodal differences. The influence of horizontal resolution was analyzed for the European Centre of Medium Range Weather Forecast numerical weather prediction model on systematic errors, cloud radiative forcing, and extratropical cyclone characteristics (Tibaldi et al., 1990; Potter, 1995; Jung et al., 2006). It was shown that low-resolution model simulations do not capture the correct nonlinear dynamics of the extratropics. Key characteristics of extratropical cyclones, that are highly sensitive to model resolution, show a tendency to more realistic patterns with increased resolution. Furthermore, cloud radiative forcing characteristics changes with model resolution. Williamson et al. (1995) conducted climate sensitivity studies with the National Center for Atmospheric Research Community Climate Model (CCM2). Their findings show large differences between low and medium resolution model versions. They conclude, that high-resolution models are required to better capture nonlinear processes of medium scales. Pope and Stratton (2002) used the Hadley Centre climate model HadAM3 to perform resolution dependent sensitivity studies. Model biases are reduced with increased model resolution. Gao et al. (2006) performed simulations with the Regional Climate Model RegCM2 and focused on changes in orography and model resolution on East Asian precipitation. The high-resolution simulation ($<$ 60 km grid) with coarse orography provides more realistic results compared to the coarse-resolution model and orography. Boville (1991) explored significant improvements in simulating the troposphere towards increased model resolutions. Hack et al. (2006) and Gent et al. (2010) performed climate sensitivity experiments with the Community Climate System Model (CCSM) Community Atmosphere Model version 3 (CAM3), and showed that biases are reduced with model resolution. Hamilton (2006) reviewed numerical model simulations with varying resolutions. Increased resolution lead to significantly overall improved global-scale circulations.

For paleoclimate conditions, experiments have been standardized and compiled by PMIP (Gladstone, 2005; Braconnot et al., 2007a, b, Brewer et al., 2007; Zheng et al., 2008; Otto-Bliesner et al., 2009, 2017, Kageyama et al., 2017; Brierley et al., 2020). Here, we supplement such intercomparisons concerning potentially resolution-dependent results. In contrast, our experimental setup is restricted here to one single model, but different resolutions under fixed boundary conditions in SST and sea ice (SI) concentration. Studies covering the Last Glacial Maximum have been presented (Rind, 1988; Dong and Valdes, 2000; Jost et al., 2005; Kim et al., 2008), while the role of model resolution in simulating glacial inception has been found by Vavrus et al. (2011). To our knowledge, no intra-model study has been performed for the Holocene epoch so far, even though the mid-Holocene (6 ka BP) is one of the most frequently simulated time slices in paleoclimate modelling and belongs to the standard PMIP experiments (e.g., Braconnot et al., 2012; Lohmann et al., 2013; Brierley et al., 2020). Compared to the Last Glacial Maximum, temperature anomalies of the mid-Holocene are much smaller, such that the ratio between model biases and simulated temperature signals is expected to be relatively large (Hargreaves et al., 2013). In this study we examine the impact of model resolution on Holocene surface temperature variations and focus on the high northern latitudes.

2. Methods

Here, we employ the atmosphere model ECHAM5 (Roeckner et al., 2003) in a stand-alone mode to isolate resolution effects on atmospheric processes in mid-Holocene simulations. The model has been tested in various resolutions (Roeckner et al., 2006) against observational datasets. Except for resolution-dependent parameter changes, the model physics remain identical. Some resolution-dependent parameters are related to the horizontal diffusion, the orographic drag scheme or the adjustment time scale in

Table 1
Overview of experiments.

Experiment		Time slices	Model grid (resolution)	Orography (resolution)
LR_{MH-PI}	LR_{MH}	MH	T31L19	T31L19
	LR_{PI}	PI	T31L19	T31L19
HR_{MH-PI}	HR_{MH}	MH	T106L31	T106L31
	HR_{PI}	PI	T106L31	T106L31
$HR_{MH-PI}(LR_{oro})$	$HR_{MH}(LR_{oro})$	MH	T106L31	T31L19
	$HR_{PI}(LR_{oro})$	PI	T106L31	T31L19

the convective parameterization (Roeckner et al., 2006).

Our experiments are summarized in Table 1, comprising the mid-Holocene (MH) and preindustrial (PI) periods. Runs were performed in two resolution modes: low (horizontal: ~3.8°, vertical: 19 levels) and high (horizontal: ~1.1°, vertical: 31 levels), referred to as $LR_{MH\text{-}PI}$ and $HR_{MH\text{-}PI}$, respectively. Boundary conditions of the used stand-alone global atmospheric model are held fixed. Furthermore, computer parallelization schemes, code and compiler structure were identical. The low-resolution version of the model (but then coupled to the ocean) has also been applied in a series of papers dealing with interglacial (Wei and Lohmann, 2012; Lohmann et al., 2013, Pfeiffer and Lohmann, 2016) as well as of the Last Glacial Maximum (Zhang et al., 2013, 2014, Werner et al., 2018) background conditions.

Greenhouse gas concentrations were adjusted to the appropriate conditions following the PMIP2 convention (Flückiger et al., 1999; Monnin et al., 2001). The varying orbital forcing parameters were computed following Berger (1978). Climatological SST and SI fields are prescribed (Fig. 1). They were derived from transient model simulations (Lorenz and Lohmann, 2004; Lohmann, 2017) performed with the coupled general circulation model ECHO-G (Legutke and Voss, 1999). The considered time period is 6000 years before present and the preindustrial period, where a climatology is obtained from an average of 100 yr, respectively. The horizonal resolution of this model is approximately 2.8° in the ocean (with equatorial refinement) and 3.8° in the atmosphere.

Furthermore, a second set of SST and SI anomalies are taken from a Holocene run (Varma et al., 2012, 2016), using the coupled general circulation model CCSM3 (Collins et al., 2006). The horizonal resolution of this model is approximately 3.0° in the ocean (with equatorial refinement) and 3.75° in the atmosphere. The climatology is obtained in the same way as explained for ECHO-G. As we do not concentrate on these four runs, we do not give additional abbreviations in the paper. These runs are shortly described in section 3.3 and are discussed subsequently.

The surface boundary conditions are used as anomalies from the reanalysis datasets provided by AMIP2 (Taylor et al., 2000). Setting up the high-resolution ECHAM5 simulations, an interpolation of SST and SI to T31 and T106 is applied (cf. Herold and Lohmann, 2009) using a first order conservative remapping by the climate data operators (Schulzweida et al., 2009).

The performed sensitivity experiments $LR_{MH\text{-}PI}$, $HR_{MH\text{-}PI}$, $HR_{MH\text{-}PI}(LR_{oro})$ are branched out into a MH and a PI time-slice run. The notation $LR_{MH\text{-}PI}$ and $HR_{MH\text{-}PI}$ capture the isolated effect of model resolution on the MH climate anomaly. In $HR_{MH\text{-}PI}(LR_{oro})$, the model has the high resolution, but the orography was replaced by a low-resolution orography in order to isolate the effect of orographic resolution on climate.

The low T31L19 (Fig. 2a) and high T106L31 (Fig. 2b) resolution orography displays similar maximum heights of mountain ranges across the Qinghai-Tibetan (Qingzang) Plateau (5201/5117 m), Greenland (3086/3055 m) and the Transantarctic Mountains (3973/3777 m). The geographic locations of these peaks and chains (T31 versus T106) are shifted up to several hundreds of kilometers, depending on the orographic resolution. Across the North and South American Cordillera, differences in altitude amount to several hundreds of meters. Resolution-dependent differences in altitude (Fig. 2) show an absolute spread of ±1600 m for the South American Cordillera, ±1300 m for the Qinghai-Tibetan (Qingzang) Plateau (due to the shift in the geolocation), ±900 m for Greenland and Antarctica and ±700 m for the North American Cordillera.

For simplicity, land surface conditions, aerosols and ozone were set to present-day conditions. For all experiments an integration time of 50 years was used, where the first 10 years were regarded as the spin-up phase and excluded from further analysis. When comparing the high-resolution with low-resolution results, we brought the low resolution to high resolution by bilinear interpolation using the climate data operators (Schulzweida et al., 2009).

3. Results

We concentrate on the Northern Hemisphere extratropics north of 40 °N. Results are presented as anomaly (MH minus PI) and anomaly difference plots where we show the summer June-July-August (JJA) and winter December-January-February (DJF) near-surface temperatures, usually described as two-meter air temperature (T2 m). The anomalies of the variables are calculated as the

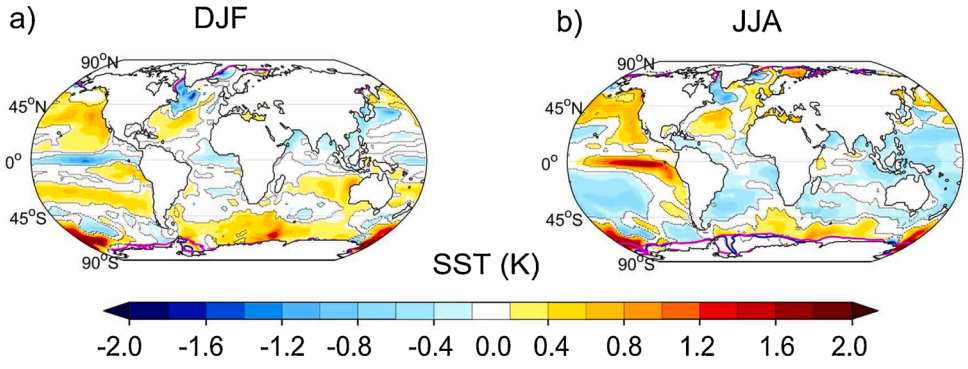

Fig. 1. SST and sea-ice concentrations for MH relative to PI based on Lorenz and Lohmann (2004). a) DJF anomaly of SST and sea-ice concentration. b) as a), but for JJA. Units are Kelvin [K]. The sea-ice 50 % concentration is marked as solid magenta (MH) and dark blue (PI) lines. Stippled lines indicate statistical significance.

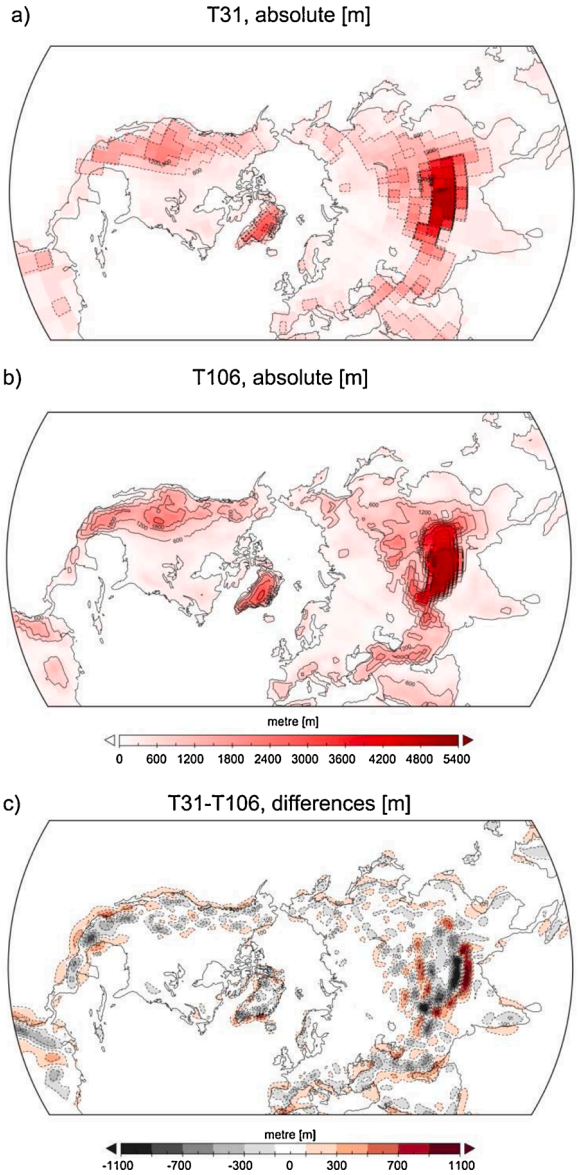

Fig. 2. Orographic height used for the performed sensitivity experiments using ECHAM5. The absolute height of the low and high-resolution model orography are shown in a) and b). Height anomalies between low (T31L19) and high (T106L31) resolution experiments are displayed in c). Units are meters [m].

mean state difference of the MH minus PI period. For significance, we apply a standard *t*-test. We show the detailed results using the ECHO-G boundary conditions in 3.1 (summer) and 3.2 (winter) for the experiments listed in Table 1, while the sensitivity experiments using CCSM3 forcing are shortly shown in 3.3.

3.1. Temperature differences for summer

For JJA, the Holocene experiments indicate a pronounced warming, especially over land (Fig. 3a–c). The low-resolution Holocene simulations ($LR_{MH\text{-}PI}$) show pronounced T2 m anomalies (Fig. 3a) as compared to $HR_{MH\text{-}PI}$ (Fig. 3b) and $HR_{MH\text{-}PI}(LR_{oro})$ (Fig. 3c) over northern Siberia and weakened warming over central Siberia and parts of North America (Fig. 3d–f). In some regions, the effect of resolution for summer T2 m (Fig. 3f) is of the same order as the Holocene T2 m anomalies (Fig. 3a,b).

The Holocene temperature anomaly differences (Fig. 3d,f) are strongly influenced by variations in shortwave cloud radiative forcing, which are in turn affected by alterations of the total cloud cover (Fig. 4a,b). Total cloud cover differences between $LR_{MH\text{-}PI}$ and $HR_{MH\text{-}PI}$ (Fig. 4a) show relative changes of $\pm$ 10 %. Differences in shortwave cloud radiative forcing (Fig. 4c) lead to JJA variations of -22 to 24 W/m^2 across Eurasia and North America. For JJA, the spatial difference patterns of the shortwave cloud forcing (Fig. 4c) and

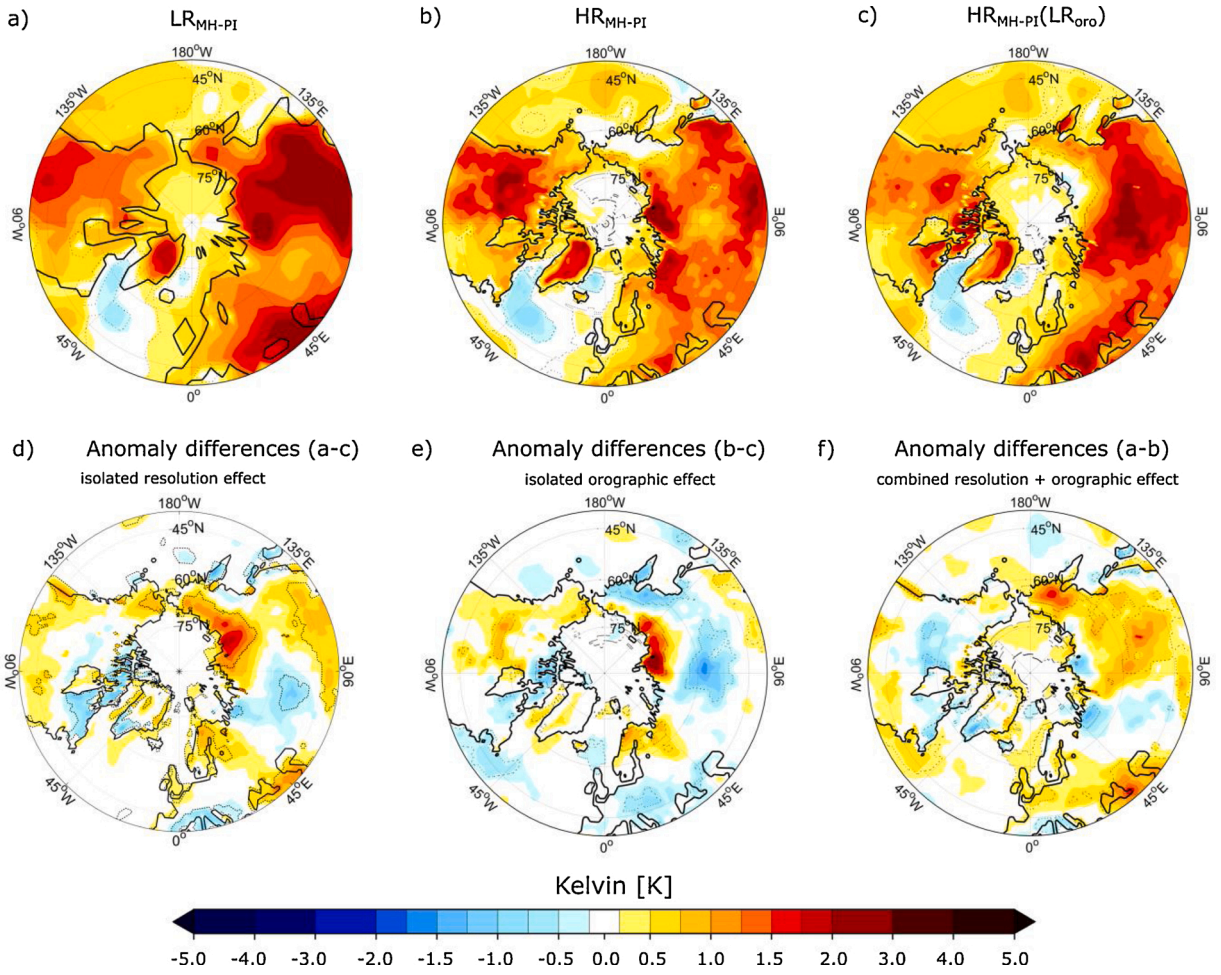

Fig. 3. Anomalous MH-PI simulated 2 m air temperature (T2 m) for JJA. a) Low- and b) high-resolution T2 m anomalies. c) High-resolution simulation with a low-resolved orography. Lower row: Resolution (d), orographic (e), and combined resolution and orographic (f) effects on MH-PI anomalies. Units are Kelvin [K]. Significant areas ($\alpha = 0.05$) are surrounded by dotted black lines. The respective coastlines are depicted by heavy solid black lines.

T2 m (Fig. 3f) are quasi-coherent and, thus, shortwave cloud forcing can be regarded as a major driving factor of the summer T2 m differences.

The isolated effect of replaced orography (fine versus coarse) shows large-scale T2 m differences in the range of $\pm$ 1 K (Fig. 3e). It is found that these T2 m differences can be accounted for by associated variations in cloud distribution (Fig. 4b), thus affecting the shortwave cloud radiative forcing balance (Fig. 4d). However, the resolution-induced T2 m differences (LR_{MH-PI} - HR_{MH-PI}; Fig. 3f) cannot be attributed solely to the changed orography (Fig. 3e).

3.2. *Temperature differences for winter*

Analogous to JJA, the DJF temperatures are shown in Fig. 5. The DJF temperature anomaly for MH minus PI in the low-resolution simulation LR_{MH-PI} is shown in Fig. 5a. Temperature anomalies range from -2.7 to 2.0 K with the largest positive anomalies in Eurasia and cold spots in eastern Siberia and over the Labrador and Greenland Seas (Fig. 5a). The high-resolution experiment HR_{MH-PI} (Fig. 5b) shows a consistent T2 m pattern across the oceanic areas. In Eurasia, the HR_{MH-PI} T2 m anomaly pattern falls into two parts with a maximum Holocene anomaly in northern Siberia and western North America (Fig. 5b). Fig. 5c shows the results of the high-resolution runs with low-resolution orography. The isolated effect of resolution arises from the difference of the low-resolution experiment LR_{MH-PI} and the high-resolution experiment with a low resolved orographic mask $HR_{MH-PI}(LR_{oro})$, as displayed in Fig. 5d.

We note that the winter T2 m anomaly differences (Fig. 5d–f) across large areas of Eurasia and North America are of the same order of magnitude as the Holocene T2 m anomalies (Fig. 5a,b). A large part of the T2 m anomaly differences can be attributed to changes in atmospheric circulation. Fig. 6 shows sea level pressure (SLP) and geopotential height at 500 hPa anomalies for LR_{MH-PI} and HR_{MH-PI}. The high-resolution experiment $HR_{MH-PI}(LR_{oro})$ with a low-resolved orographic mask is displayed in Fig. 6c. The lower row shows the

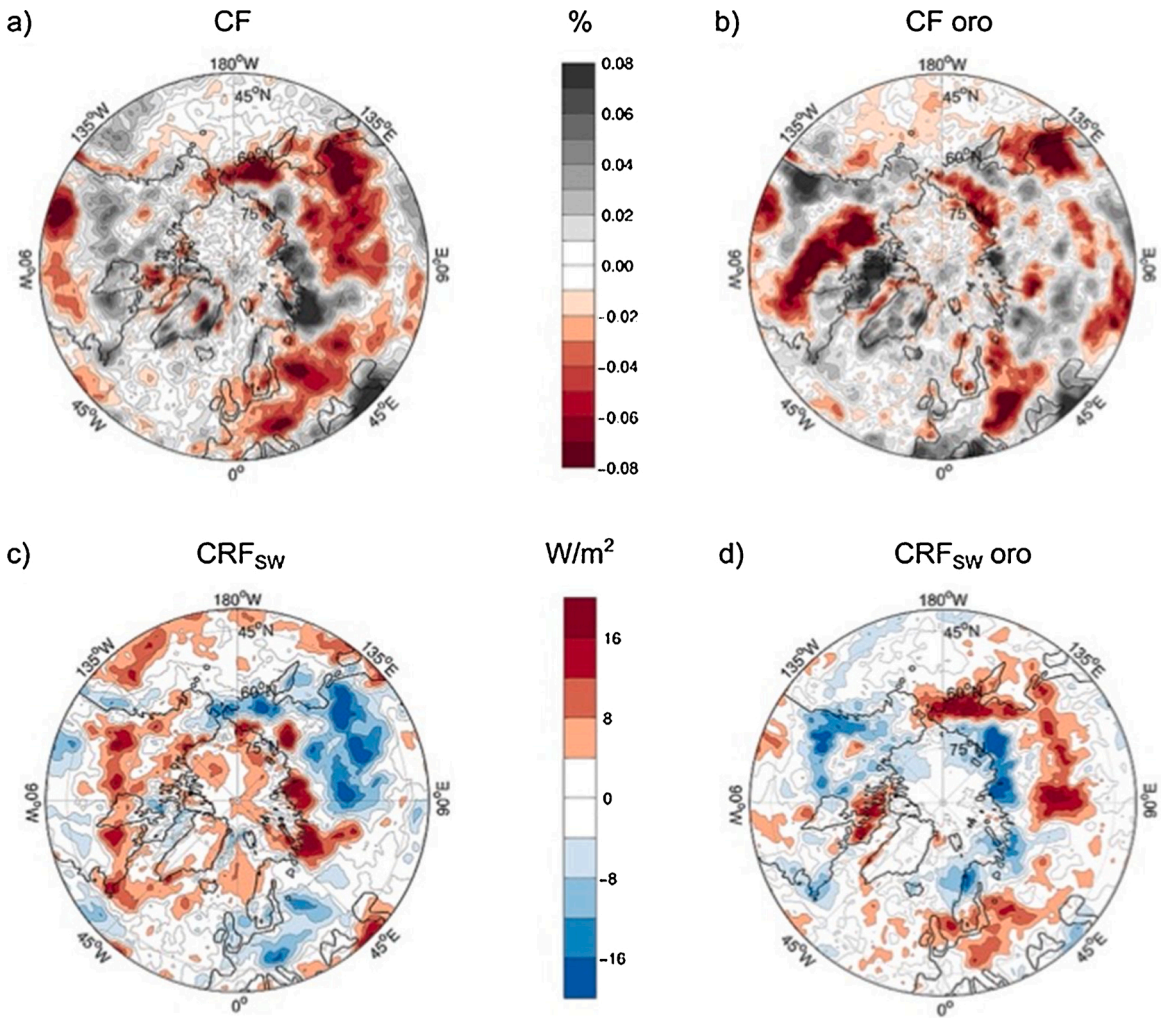

Fig. 4. Differences of total cloud cover (CF) (a,b) and shortwave surface cloud radiative forcing (CRF_{sw}) (c,d) for JJA. a,c) Difference between experiment LR_{MH-PI} and HR_{MH-PI}. b,d) Difference between HR_{MH-PI} and $HR_{MH-PI}(LR_{oro})$. Units are percentages [%]/100 for CF and Watts per square meter [W/m^2] for CRF_{sw}. For lines see caption of Fig. 3.

associated geopotential height anomalies at 500 hPa. In LR_{MH-PI}, the circulation bears similarities with the Arctic Oscillation pattern. The low-pressure center in Fig. 6a yields a pronounced warming over Eastern Europe and part of Siberia (Fig. 5a).

In HR, the anomalous SLP pattern has a wave-like structure (Fig. 6b), and is responsible for the heterogenous warming in the northern part of Siberia and eastern North America (Fig. 5b). A pronounced low-pressure anomaly over northern North America (Fig. 6b) is associated to the advection of air from the East Pacific Ocean to central North America, creating a positive T2 m anomaly in HR_{MH-PI} (Fig. 5b). A lowering in surface albedo (max. 10 %) due to snow cover reduction amplifies the T2 m changes (not shown).

As a response to the different orography, the geopotential height field mirrors a strong barotropic response across the Northern Hemisphere (Fig. 6c,f). The stationary wave pattern (Fig. 6e) is transformed substantially (Fig. 6f). The T2 m anomalies show a heterogenic pattern across eastern North America and several regions of Eurasia (Fig. 5a,b). The differences between HR_{MH-PI} and LR_{MH-PI} (Fig. 5f) are in the same order of magnitude as the respective Holocene anomalies (Fig. 5a,b). The HR experiment with low-resolution orography on the other side shows a distinct pattern with no clear relation of SLP and T2 m anomaly (Figs. 5c and 6 c).

3.3. Temperature differences with another set of lower boundary conditions

Finally, we show the changes in MH temperatures by using another background SST and SI as obtained by Varma et al. (2012, 2016). Fig. 7a,b shows the forcing fields, and Fig. 7c,d the respective boreal summer and winter MH-PI anomalies for the low-resolution simulation LR_{MH-PI}. Temperature anomalies range from -2 to 2 K with the largest positive anomalies in eastern Siberia (Fig. 7c) for boreal summer and largest negative anomalies over North America (Fig. 7d) for boreal winter.

The relative anomalies of the high-resolution experiments show pronounced heterogenous cold and warm spots of up to 2 K (Fig. 7e) for boreal summer and large-scale differences in boreal winter (Fig. 7f). This is again related to a substantial change in

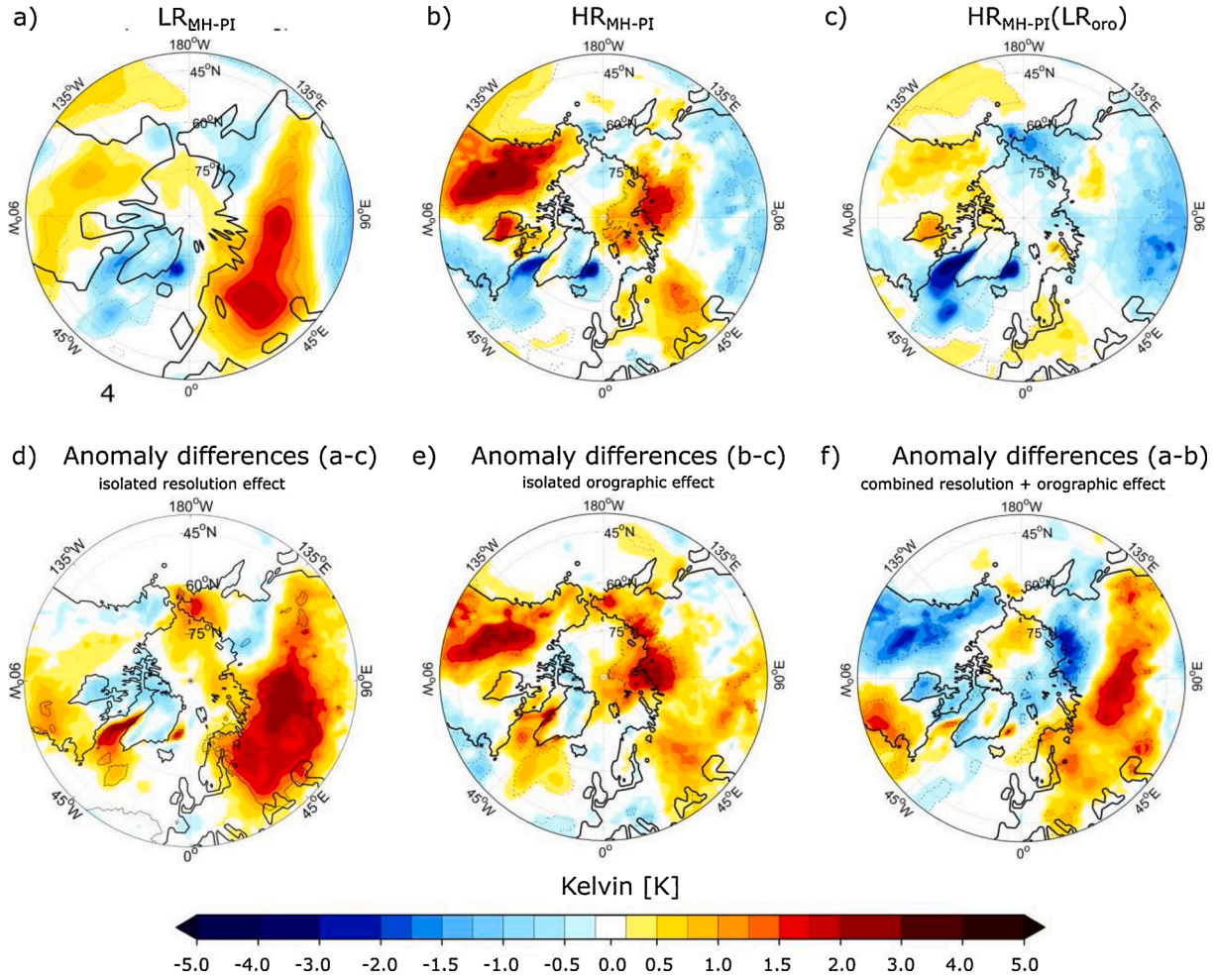

Fig. 5. As Fig. 3, but for DJF.

atmospheric circulation (not shown). We have not performed the high-resolution runs with low-resolution orography LR$_{MH-PI}$(LR$_{oro}$) using the SST and SI of Varma et al. (2012, 2016).

4. Discussion

A set of mid-Holocene sensitivity experiments was carried out with the atmospheric general circulation model ECHAM5. Each experiment was performed in two resolution modes: low (~3.75°, 19 vertical levels) and high (~1.1°, 31 vertical levels), and prescribed SST and sea ice distributions using output from coupled climate models were applied. Furthermore, we performed an additional experiment where the high-resolution orography was replaced by the coarse orography in order to isolate the effect of orographic resolution on the climate simulation. We emphasize that boundary conditions over the ocean are deliberately held fixed in order to isolate the effect for the atmosphere. This is in contrast to previous studies, where we changed the resolution in the ocean and atmosphere for early and mid-Holocene experiments (Shi and Lohmann, 2016; Shi et al., 2020) and found that the simulated mean climates show significant differences with different model resolutions. As the model versions are not available for arbitrary resolutions, we cannot evaluate whether the resolution effect is due to the changed horizontal or vertical resolution.

As a consequence of increased grid resolution in climate models, more accurate simulations of physical processes on a more local scale are expected. Low-resolution model results are now complemented by higher-resolved simulations and are often compared with each other in model intercomparison studies like PMIP. The resolution dependence in numerical simulations is thus of particular interest. The mid-Holocene is one of the key times in the past to test models (e.g., Braconnot et al., 2012; Otto-Bliesner et al., 2017). The most prominent difference between the mid-Holocene and present day arises from the orbital configuration, which leads to an increase in boreal summer insolation in the Northern Hemisphere and a decrease in the tropical and subtropical Southern Hemisphere in boreal winter. In several model simulations we test if the resolution of the atmospheric component can affect the results where we concentrate on the Northern Hemisphere.

Our summer temperature distribution across Eurasia and North America is in agreement with earlier results published in PMIP

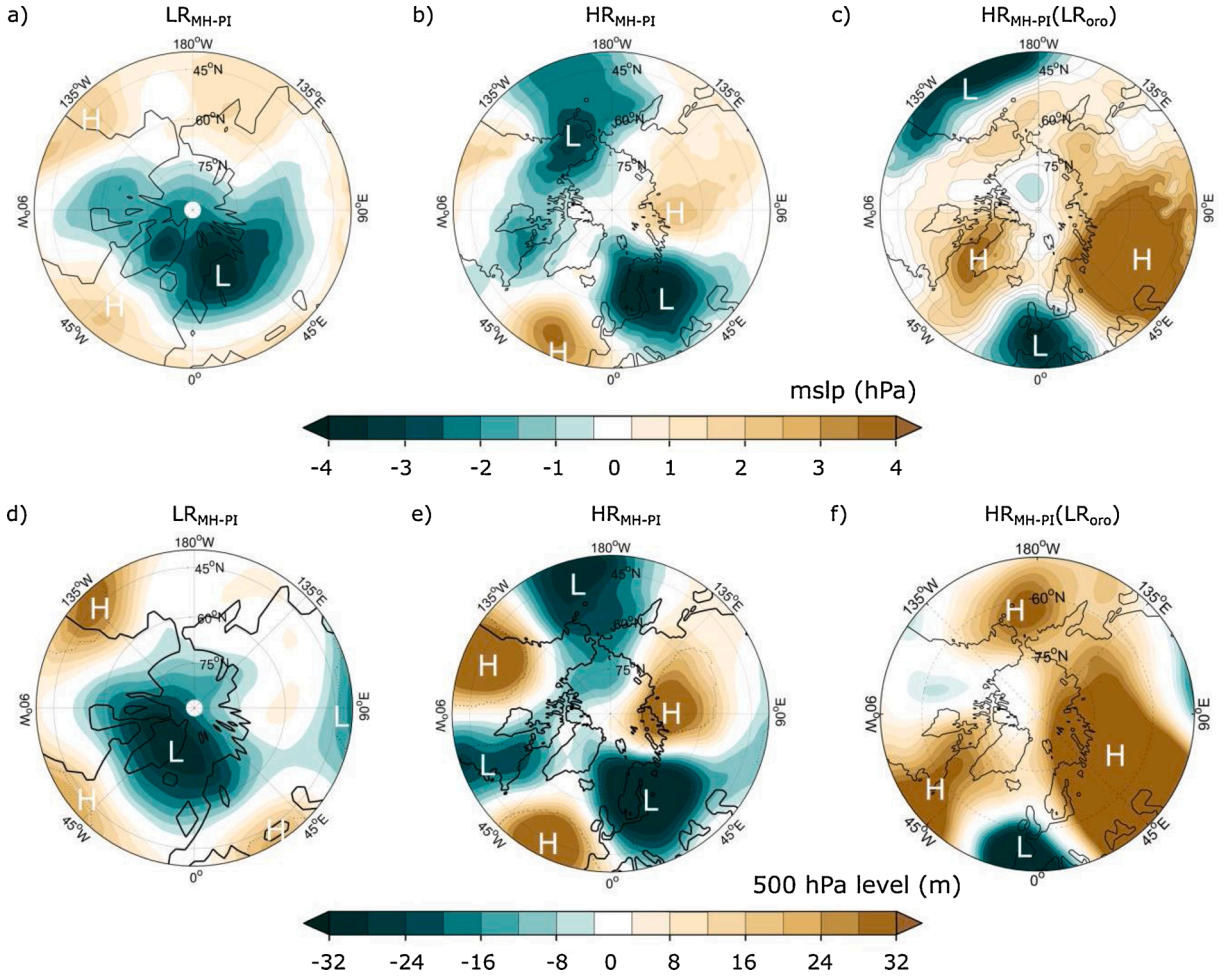

Fig. 6. Sea level pressure (upper row) and geopotential height at 500 hPa (lower row) anomalies (MH minus PI) for DJF. Units of sea level pressure are in hectoPascal [hPa] and for geopotential height in meters [m].

(Braconnot et al., 2007a, 2012; Lohmann et al., 2013). These simulations (ensemble median) capture a mid-to-late Holocene cooling trend of summer surface temperatures over continental Eurasia and North America with a maximum of 2 K. Increases in total cloud cover were found to contribute to these changes (Braconnot et al., 2007b, 2012). On the regional scale, T2 m anomaly differences of LR_{MH-PI} minus HR_{MH-PI} are above the summer differences between MH and PI (Fig. 3f). Here, the low-resolution simulations show higher total cloud cover distribution over Eurasia and North America as compared to the high-resolved simulations. Annual mean differences exceed 15 % on a regional scale, seasonal differences surpass 35 %. The cloud cover differences in turn affect the cloud radiation balance. Nam and Quaas (2012) describe this phenomenon while evaluating ECHAM5 simulations by satellite datasets. They demonstrate that ECHAM5 underestimates cloud radiative forcing when total cloud coverage is large. The downstream process influences the evaporation and hence the water cycle in the model as well. Dimri (2004) and Giorgi and Marinucci (1996) point out the sensitivity of physical parameterizations in climate models as a function of their horizontal resolution. For ECHAM5, the subgrid-scale cloud scheme depends on the represented model resolution (Roeckner et al., 2003, 2006). Thus, variations in total cloud cover between varying model versions are associated with modified parameters in the cloud and convective schemes. The resolution-dependent differences of these variables lead to changes in surface temperature (Roeckner et al., 2006, Dallmeyer, 2008). This feature can be highly model-dependent.

For DJF, the combined effect of resolution and orography (LR_{MH-PI} minus HR_{MH-PI}) is more pronounced (Fig. 5f) and thus surpasses MH temperature changes throughout large areas of continental Eurasia and North America. The sensitivity study HR_{MH-PI} (LR_{oro}) represents the isolated effect of orographic-induced T2 m anomalies. Pronounced T2 m anomaly differences during DJF are reflected across northern Eurasia and western and central North America (Fig. 5e). The results are in line with the findings of Charney and Eliassen (1949); Grose and Hoskins (1979), and Hoskins and Karoly (1981). They argued that mountain barriers of the size of the Rocky Mountains and the Himalayas influence the position of the stationary Rossby wave. Kasahara (1966); Kasahara et al. (1973), and Manabe and Terpstra (1974) applied atmospheric general circulation models to isolate the effect of mountain ranges and planetary waves. They ran a set of simulations with and without the effect of mountains and focused on the stationary and transient disturbance

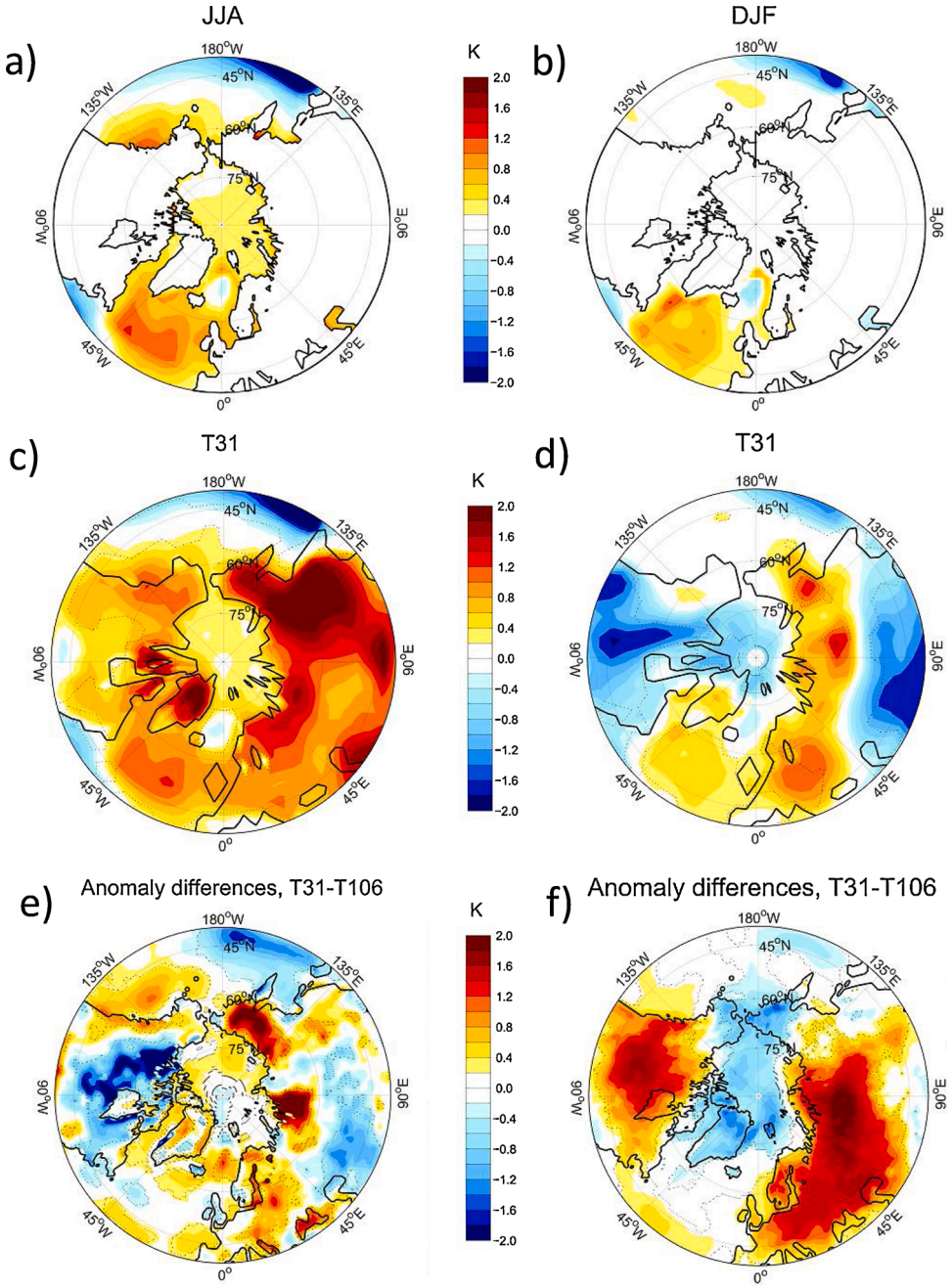

Fig. 7. a,b) Mid-Holocene SST anomalies [K] based on CCSM3 simulations of Varma et al. (2016). Anomalies MH-PI of T2 m for JJA (c) and DJF (d) for the low-resolution ECHAM5 simulation. The difference between the high- and low-resolution simulations (e,f). Stippled lines as in Fig. 3.

of atmospheric wave trains. The presence of mountain barriers led to an increase in the stationary component of the eddy conversion while the absence of mountains causes the opposite. Furthermore, Manabe et al. (1970) reported in an earlier study that the resolution of the orographic mask and model do play an important role to this phenomenon.

Orographic effects during JJA are of minor influence to T2 m anomaly changes (Fig. 3e). The effects of orographic resolution and clouds are identified for both boreal summer and winter, whereby during DJF the effects are more pronounced (Figs. 3f and 5 f). Furthermore, snow cover and surface albedo across the Rocky Mountain Range and central North America act as an amplifying mechanism to temperature changes. The isolated effect of orography in $HR_{MH\text{-}PI}(LR_{oro})$ shows temperature anomalies during boreal winter that are seen in the immediate vicinity of large-scale mountain ranges. Our $LR_{MH\text{-}PI}$ minus $HR_{MH\text{-}PI}$ and $HR_{MH\text{-}PI}(LR_{oro})$ results indicate resolution-induced temperature anomalies that are regionally as large as the MH temperature anomalies. In particular, $HR_{MH\text{-}PI}(LR_{oro})$ shows that the effect of the low resolution of orography cannot explain the differences in $LR_{MH\text{-}PI}$ and $HR_{MH\text{-}PI}$. The interaction

between orography and MH thermal forcing leads to characteristic stationary wave patterns.

Our results have implications for data-model comparisons. We emphasize, however, that a detailed data-model comparison is beyond the scope of the present paper. Comparing our DJF temperature anomalies (LR_{MH-PI} versus HR_{MH-PI}) with proxy data (e.g., Bartlein et al., 2011), we do not see a clear increase in the performance in HR_{MH-PI} relative to LR_{MH-PI} (Figs. 5 and 7). Proxy data suggest a reduced latitudinal temperature gradient over Europe during the mid-Holocene (Bartlein et al., 2011) which is more pronounced in HR_{MH-PI} than in LR_{MH-PI}. Across West Siberia proxy and model data show similar positive Holocene temperature anomalies. Across Central Eurasia, the low-resolution model experiments better reflect the positive MH temperature anomalies, compared with the negative T2 m anomaly of the higher resolved version. The T2 m anomaly differences between the model runs are strongest over Siberia and the Rocky Mountain Range. In the area of the Rocky Mountain Range, pollen data (Viau et al., 2006; Bartlein et al., 2011, Kaufman et al., 2020) and model experiments show contrasting anomalies (pollen negative vs. model positive). Our MH results confirm the general statement that current models have a limited ability to reproduce spatial patterns of reconstructed temperature changes (e. g., Harrison et al., 2014).

For JJA T2 m anomalies (Figs. 3 and 7), low- and high-resolution model runs show continental-wide positive temperature anomalies during the mid-Holocene. Higher MH T2 m compared to PI (Fig. 3a,b) over Europe and northern Siberia are consistent with multi-proxy reconstructions of the northern high-latitudes (Sundqvist et al., 2010, Kaufman et al., 2020) as well as specific pollen and plant macrofossil records (Prentice et al., 1996; Tarasov et al., 1998; MacDonald et al., 2000; Seppä and Birks, 2001). A southward retreat of Arctic treelines is related to a decline in Arctic mid-to-late Holocene summer temperatures. Lake records from western Greenland estimate local MH summer temperatures of approximately 2–3 K higher than present day (Axford et al., 2013). $\delta^{18}O$ records in ice cores from the Agassiz Ice Cap on Ellesmere Island imply a summer cooling of 4 K from 8 ka BP to present (Fisher et al., 1995). Briner et al. (2016) report that temperatures of Arctic Canada and Greenland decreased by approximately 3 ± 1 K from the mid-to-late Holocene.

5. Conclusions

The resolution dependence of model results has been addressed for present day conditions (e. g. Jost et al., 2005; Hack et al., 2006; Roeckner et al., 2006; Byrkjedal et al., 2008; Kim et al., 2008). The studies point out the benefits of higher resolved model experiments. However, Harrison et al. (2015) pointed out that differences in performance can only weakly be related to modern-day biases, and more sophisticated models are not necessarily better at simulating climate changes. Therefore, an understanding of MH climate dynamics is essential. Our mid-Holocene climate simulations with ECHAM5 demonstrate the dependence of continental surface air temperatures on spatial resolution and orography changes. When comparing the different resolutions, we see that on the regional scale temperature anomaly differences can be of the same order of magnitude as simulated MH temperature anomalies. Differences in boreal winter temperature anomalies are largely attributable to distinct stationary wave patterns. We suspect that stationary and transient eddies and the model's climatological basic states determine the atmospheric response to MH thermal forcing anomalies, in a similar way as described in other contexts (e.g., Chervin et al., 1980; Held et al., 2002; Branstator, 2002; Kushnir et al., 2002; Brandefelt and Kornich, 2008; Branstator and Selten, 2009). Meridionally trapped waves of this kind have been seen in other contexts, where they have been termed "circum-global waves" (Branstator, 2002), consisting of an equivalent barotropic wave. In contrast, the summer temperature differences between the low- and high-resolution models can be largely attributed to changes in shortwave cloud radiative forcing which is consistent with the finding that the shortwave cloud feedback is a major driver of differences between PMIP model results, highlighting the fingerprint of model physics (Braconnot and Kageyama, 2015).

In all experiments, SST and sea ice fields remained fixed and thus, we isolate the effect in atmosphere-only experiments. This advantage of fixed SSTs constitutes at the same time a disadvantage, since the SSTs cannot develop freely and are not completely consistent with the atmospheric circulation pattern, because the circulation would affect SST and sea ice. This can be directly seen in our set up. The original ECHO-G simulation showed a pronounced Arctic Oscillation-like response for the MH winter (Lorenz and Lohmann, 2004; Felis et al., 2004; Lohmann, 2017), whereas the atmospheric circulation forced by the output of this particular simulation shows a different atmospheric response for the high-resolution version. Furthermore, the response of low- and high-resolution versions differ considerably when using other mid-Holocene lower boundary conditions. As a logical next step, we will perform simulations by using different background climates as derived from PMIP (e.g. Brierley et al., 2020). Our experiments using different background SST and sea ice might be a starting point for more systematic analyses of the system.

Our results imply that differences in paleoclimate simulations could partly be attributed to the use of different resolutions, even when using the same atmospheric circulation model. It is conceivable that high-resolution models are required to represent the atmospheric dynamics such as baroclinic waves and even blocking phenomena (e. g. D'Andrea et al., 1996; Matsueda et al., 2009; Scaife et al., 2010; Berckmans et al., 2013; Dunn-Sigouin and Son, 2013; Rimbu et al., 2014). Blockings play a central role for the extratropical circulation, mean climate and extremes (Masato et al., 2013, Ionita et al., 2016, Lutsko et al., 2019). Related to this, persistent episodes of extreme weather in the Northern Hemisphere summer were associated with the presence of high-amplitude quasi-stationary atmospheric Rossby waves within a particular wavelength range becoming trapped within an effective mid-latitude atmospheric waveguide (Branstator, 2002; Mann et al., 2017; Wills et al., 2019). Therefore, high-resolution models are most likely necessary to resemble the decadal to millennial variability as seen in the paleorecords (Laepple and Hubers, 2014; Lohmann et al., 2020). Future work shall examine the potential of using high-resolution modelling to infer the variability and frequency of past extremes (Petoukhov et al., 2013). For intercomparison studies, we suggest future studies to systematically explore resolution-dependent results in coupled and uncoupled general circulation models.

Author statement

Please find enclosed our revised paper submitted to "Dynamics of Atmospheres and Oceans".

Prof. Dr. Gerrit Lohmann
Alfred Wegener Institute
Helmholtz Centre for Polar and Marine Research
Bussestr. 24
Bremerhaven
Germany
Gerrit.Lohmann@awi.de
http://paleodyn.uni-bremen.de/

Author contributions

All authors contributed to the analysis and writing of the manuscript. GL and MP lead the project and paper writing, AW performed simulations and wrote part of an earlier version of the manuscript.

Code availability

The standard model code is based on the Community Earth System Models version COSMOS-landveg r2413 (2009) and is available upon request from the Max Planck Institute for Meteorology in Hamburg (https://www.mpimet.mpg.de).

Declaration of Competing Interest

The authors declare that they have no known competing financial interests or personal relationships that could have appeared to influence the work reported in this paper.

Acknowledgements

This research work has been supported by the German Research Foundation (DFG), project ID: LO 895/13-1, PR 1050/3-1, and BMBF projects PalMod and PACMEDY. Model integrations were carried out with computer facilities provided by the Alfred Wegener Institute for Polar and Marine Research. AMIP Reanalysis data has been provided by the NOAA/OAR/ESRL PSD, Boulder, Colorado, USA, from their Web site (http://www.esrl.noaa.gov/psd/). Thanks go to the Max Planck Institute for Meteorology in Hamburg for providing the model code. Thanks go to Stephan Lorenz and Vidya Varma for providing model output. The manuscript benefited from constructive comments of three anonymous referees, as well as proofreading from Wally.

References

Axford, Y., Losee, S., Briner, J.P., Francis, D.R., Langdon, P.G., Walker, I.R., 2013. Holocene temperature history at the western Greenland Ice Sheet margin reconstructed from lake sediments. Quat. Sci. Rev. 59, 87–100.

Bader, D.C., Covey, C., Gutkowski Jr., W.J., I. M. H, Kunkel, K.E., Miller, R.L., Tokmakian, R.T., Zhang, M.H., 2008. Climate Models: An Assessment of Strengths and Limitations, 124 pp..

Bartlein, P., Harrison, S., Brewer, S., Connor, S., Davis, B., Gajewski, K., Guiot, J., Harrison-Prentice, T., Henderson, A., Peyron, O., Prentice, I., Scholze, M., Seppä, H., Shuman, B., Sugita, S., Thompson, R., Viau, A., Williams, J., Wu, H., 2011. Pollen-based continental climate reconstructions at 6 and 21 ka: a global synthesis. Clim. Dyn. 37 (3), 775–802.

Berckmans, J., Woollings, T., Demory, M.-E., Vidale, P.-L., Roberts, M., 2013. Atmospheric blocking in a high resolution climate model: influences of mean state, orography and eddy forcing. Atmos. Sci. Lett. 14 (1), 34–40.

Berger, A., 1978. Long-term variations of daily insolation and quaternary climatic changes. J. Atmos. Sci. 35 (12), 2362–2367.

Bolin, B., 1950. On the influence of the earth's orography on the general character of the westerlies. Tellus 2 (3), 184–195.

Boville, B.A., 1991. Sensitivity of simulated climate to model resolution. J. Clim. 4 (5), 469–485.

Braconnot, P., Kageyama, M., 2015. Shortwave forcing and feedbacks in last glacial maximum and mid-holocene PMIP3 simulations. Philos. Trans. R. Soc. A 373, 20140424. https://doi.org/10.1098/rsta.2014.0424.

Braconnot, P., Otto-Bliesner, B., Harrison, S., Joussaume, S., Peterchmitt, J.Y., Abe-Ouchi, A., Crucifix, M., Driesschaert, E., Fichefet, T., Hewitt, C.D., Kageyama, M., Kitoh, A., Laîné, A., Loutre, M.F., Marti, O., Merkel, U., Ramstein, G., Valdes, P., Weber, S.L., Yu, Y., Zhao, Y., 2007a. Results of PMIP2 coupled simulations of the Mid-Holocene and Last Glacial Maximum; Part 1: experiments and large-scale features. Clim. Past 3 (2), 261–277.

Braconnot, P., Otto-Bliesner, B., Harrison, S., Joussaume, S., Peterchmitt, J.Y., Abe-Ouchi, A., Crucifix, M., Driesschaert, E., Fichefet, T., Hewitt, C.D., Kageyama, M., Kitoh, A., Loutre, M.F., Marti, O., Merkel, U., Ramstein, G., Valdes, P., Weber, L., Yu, Y., Zhao, Y., 2007b. Results of PMIP2 coupled simulations of the Mid-Holocene and Last Glacial Maximum - Part 2: feedbacks with emphasis on the location of the ITCZ and mid- and high latitudes heat budget. Clim. Past 3 (2), 279–296.

Braconnot, P., Harrison, S.P., Kageyama, M., Bartlein, P.J., Masson-Delmotte, V., Abe-Ouchi, A., Otto-Bliesner, B., Zhao, Y., 2012. Evaluation of climate models using palaeoclimatic data. Nat. Clim. Change 2, 417–424.

Brandefelt, J., Kornich, H., 2008. Northern Hemisphere stationary waves in future climate projections. J. Clim. 21, 6341–6353. https://doi.org/10.1175/2008JCLI2373.1.

Branstator, G., 2002. Circumglobal teleconnections, the jet stream waveguide, and the North Atlantic Oscillation. J. Clim. 15, 1893–1910. https://doi.org/10.1175/1520-0442(2002)015<1893:CTTJSW>2.0.CO;2.

Branstator, G., Selten, F., 2009. "Modes of variability" and climate change. J. Clim. 22, 2639–2658. https://doi.org/10.1175/2008JCLI2517.1.

Brewer, S., Guiot, J., Torre, F., 2007. Mid-Holocene climate change in Europe: a data-model comparison. Clim. Past 3, 499–512.

Brierley, C.M., Zhao, A., Harrison, S.P., Braconnot, P., Williams, C.J.R., Thornalley, D.J.R., Shi, X., Peterschmitt, J.-Y., Ohgaito, R., Kaufman, D.S., Kageyama, M., Hargreaves, J.C., Erb, M.P., Emile-Geay, J., D'Agostino, R., Chandan, D., Carré, M., Bartlein, P., Zheng, W., Zhang, Z., Zhang, Q., Yang, H., Volodin, E.M., Tomas, R.A., Routson, C., Peltier, W.R., Otto-Bliesner, B., Morozova, P.A., McKay, N.P., Lohmann, G., Legrande, A.N., Guo, C., Cao, J., Brady, E., Annan, J.D., Abe-Ouchi, A., 2020. Large-scale features and evaluation of the PMIP4-CMIP6 midHolocene simulations. Clim. Past 16, 1847–1872. https://doi.org/10.5194/cp-16-1847-2020.

Briner, J.P., McKay, N.P., Axford, Y., Bennike, O., Bradley, R.S., de Vernal, A., Fisher, D., Francus, P., Fréchette, B., Gajewski, K., Jennings, A., Kaufman, D.S., Miller, G., Rouston, C., Wagner, B., 2016. Holocene climate change in Arctic Canada and Greenland. Quat. Sci. Rev. 147, 340–364.

Byrkjedal, Ø., Esau, I., Kvamstø, N., 2008. Sensitivity of simulated wintertime Arctic atmosphere to vertical resolution in the ARPEGE/IFS model. Clim. Dyn. 30 (7), 687–701.

Cess, R.D., Potter, G.L., Blanchet, J.P., Boer, G.J., Del Genio, A.D., qu, M., Dymnikov, V., Galin, V., Gates, W.L., Ghan, S.J., Kiehl, J.T., Lacis, A.A., Le Treut, H., Li, Z.X., Liang, X.Z., McAvaney, B.J., Meleshko, V.P., Mitchell, J.F.B., Morcrette, J.J., Randall, D.A., Rikus, L., Roeckner, E., Royer, J.F., Schlese, U., Sheinin, D.A., Slingo, A., Sokolov, A.P., Taylor, K.E., Washington, W.M., Wetherald, R.T., Yagai, I., Zhang, M.H., 1990. Intercomparison and interpretation of climate feedback processes in 19 atmospheric general circulation models. J. Geophys. Res. 95 (D10), 16601–16615.

Charney, J.G., Eliassen, A., 1949. A numerical method for predicting the perturbations of the middle latitude westerlies. Tellus 1 (2), 38–54.

Chervin, R.M., Kutzbach, J.E., Houghton, D.D., Gallimore, R.G., 1980. Response of the NCAR general circulation model to prescribed changes in ocean surface temperature. Part II: midlatitude and subtropical changes. J. Atmos. Sci. 37 (2), 308–332.

Collins, W.D., Bitz, C.M., Blackmon, M.L., Bonan, G.B., Bretherton, C.S., Carton, J.A., Chang, P., Doney, S.C., Hack, J.J., Henderson, T.B., Kiehl, J.T., Large, W.G., McKenna, D.S., Santer, B.D., Smith, R.D., 2006. The community climate system model version 3 (CCSM3). J. Clim. 19 (11), 2122–2143.

Cook, K.H., Held, I.M., 1992. The stationary response to large-scale orography in a general circulation model and a linear model. J. Atmos. Sci. 49 (6), 525–539.

Cubasch, U., Meehl, G.A., Boer, G.J., Stouffer, R.J., Dix, M., Noda, A., Senior, C.A., Raper, S., Yap, K.S., Abe-Ouchi, A., Brinkop, S., Claussen, M., Collins, M., Evans, J., Fischer-Bruns, I., Flato, G.M., Fyfe, J.C., Ganopolski, A., Gregory, J.M., Hu, Z.-Z., Joos, F., Knutsen, T., Knutti, R., Landsea, C., Mearns, L., Milly, C., Mitchell, J.F.B., Nozawa, T., Paeth, H., Räisänen, J., Sausen, R., Smith, S., Stocker, T., Timmermann, A., Ulbrich, U., Weaver, A.J., Wegner, J., Whetton, P., Wigley, T.M.L., Winton, M., Zwiers, F.W., 2001. Projections of future climate change. In: Houghton, J.T., Ding, Y., Griggs, D.J., Noguer, M., van der Linden, P.J., Dai, X., Maskell, K., Johnson, C.A. (Eds.), Climate Change 2001: The Scientific Basis. Cambridge University Press, pp. 525–582.

D'Andrea, F., Tibaldi, S., Blackburn, M., Boer, G., Deque, M., Dix, M.R., Dugas, B., Ferranti, L., Iwasaki, T., Kitoh, A., Pope, V., Randall, D., Roeckner, E., Straus, D., Stern, W., Van den Dool, H., Williamson, D., 1996. Northern Hemisphere atmospheric blocking as simulated by 15 atmospheric general circulation models in the period 1979-1988 (Results from an AMIP diagnostic subproject). Geneva Rep. 14, 385–407.

Dallmeyer, A., 2008. Simulation des Nordafrikanischen Sommermonsuns in ECHAM5. Analyse der Modellempfindlichkeit, Fachbereich Geowissenschaften, Master thesis. Universität Hamburg, Hamburg, Germany, 103 pp.

Dimri, A.P., 2004. Impact of horizontal model resolution and orography on the simulation of a western disturbance and its associated precipitation. Meteorol. Appl. 11 (2), 115–127.

Dong, B., Valdes, P.J., 2000. Climates at the last glacial maximum: influence of model horizontal resolution. J. Clim. 13 (9), 1554–1573.

Dunn-Sigouin, E., Son, S.-W., 2013. Northern Hemisphere blocking frequency and duration in the CMIP5 models. J. Geophys. Res. Atmos. 118 (3), 1179–1188.

Felis, T., Lohmann, G., Kuhnert, H., Lorenz, S., Scholz, D., Pätzold, J., Al-Rousan, S.A., Al-Moghrabi, S.M., 2004. Increased seasonality in Middle East temperatures during the last interglacial period. Nature 429, 164–168.

Fisher, D.A., Koerner, R.M., Reeh, N., 1995. Holocene climatic records from Agassiz Ice Cap, Ellesmere Island, NWT, Canada. Holocene 5 (1), 19–24.

Flato, G., Marotzke, J., Abiodun, B., Braconnot, P., Chou, S.C., Collins, W., Cox, P., Driouech, F., Emori, S., Eyring, V., Forest, C., Gleckler, P., Guilyardi, E., Jakob, C., Kattsov, V., Reason, C., Rummukainen, M., 2013. Evaluation of climate models. In: Stocker, T.F., Qin, D., Plattner, G.-K., Tignor, M., Allen, S.K., Boschung, J., Nauels, A., Xia, Y., Bex, V., Midgley, P.M. (Eds.), Climate Change 2013: The Physical Science Basis. Contribution of Working Group I to the Fifth Assessment Report of the Intergovernmental Panel on Climate Change. Cambridge University Press, Cambridge, United Kingdom and New York, NY, USA, pp. 741–866.

Flückiger, J., Dällenbach, A., Blunier, T., Stauffer, B., Stocker, T.F., Raynaud, D., Barnola, J.-M., 1999. Variations in atmospheric N_2O concentration during abrupt climatic changes. Science 285 (5425), 227–230.

Gao, X., Xu, Y., Zhao, Z., Pal, J.S., Giorgi, F., 2006. On the role of resolution and topography in the simulation of East Asia precipitation. Theor. Appl. Climatol. 86 (1), 173–185.

Gent, P., Yeager, S., Neale, R., Levis, S., Bailey, D., 2010. Improvements in a half degree atmosphere/land version of the CCSM. Clim. Dyn. 34 (6), 819–833.

Giorgi, F., Marinucci, M.R., 1996. A investigation of the sensitivity of simulated precipitation to model resolution and its implications for climate studies. Mon. Weather. Rev. 124 (1), 148–166.

Gladstone, R.M., 2005. Mid-Holocene NAO: a PMIP2 model intercomparison. Geophys. Res. Lett. 32 (16), L16707.

Grose, W.L., Hoskins, B.J., 1979. On the influence of orography on large-scale atmospheric flow. J. Atmos. Sci. 36 (2), 223–234.

Hack, J.J., Caron, J.M., Danabasoglu, G., Oleson, K.W., Bitz, C., Truesdale, J.E., 2006. CCSM–CAM3 climate simulation sensitivity to changes in horizontal resolution. J. Clim. 19 (11), 2267–2289.

Hamilton, K., 2006. High resolution global modeling of the atmospheric circulation. Adv. Atmos. Sci. 23 (6), 842–856.

Harrison, S.P., Bartlein, P.J., Prentice, I.C., Boyd, M., Hessler, I., Holmgren, K., Isumi, K., Willis, K., 2014. Climate model benchmarking with glacial and mid-Holocene climates. Clim. Dyn. 43 (3–4), 671–688.

Harrison, S., Bartlein, P., Izumi, K., Li, G., Annan, J., Hargreaves, J., Braconnot, P., 2015. Evaluation of CMIP5 palaeo-simulations to improve climate projections. Nat. Clim. Change 5, 735–743.

Held, I.M., Ting, M., Wang, H., 2002. Northern winter stationary waves: theory and modeling. J. Clim. 15 (16), 2125–2144.

Herold, M., Lohmann, G., 2009. Eemian tropical and subtropical African moisture transport: an isotope modelling study. Clim. Dyn. 33 (7), 1075–1088.

Hoskins, B.J., Ambrizzi, T., 1993. Rossby wave propagation on a realistic longitudinally varying flow. J. Atmos. Sci. 50 (12), 1661–1671.

Hoskins, B.J., Karoly, D., 1981. The steady linear response of a spherical atmosphere to thermal and orographic forcing. J. Atmos. Sci. 38 (6), 1179–1196.

Houghton, D.D., Kutzbach, J.E., McClintock, M., Suchman, D., 1974. Response of a general circulation model to a sea temperature perturbation. J. Atmos. Sci. 31 (4), 857–868.

Huang, J.C.K., 1978. Response of the NCAR general circulation model to North Pacific Sea surface temperature anomalies. J. Atmos. Sci. 35 (7), 1164–1179.

Ionita, M., Scholz, P., Lohmann, G., Dima, M., Prange, M., 2016. Linkages between atmospheric blocking, sea ice export through Fram Strait and the Atlantic Meridional Overturning Circulation. Scientific Reports 6, 32881. https://doi.org/10.1038/srep32881.

Jost, A., Lunt, D., Kageyama, M., Abe-Ouchi, A., Peyron, O., Valdes, P., Ramstein, G., 2005. High-resolution simulations of the last glacial maximum climate over Europe: a solution to discrepancies with continental palaeoclimatic reconstructions? Clim. Dyn. 24 (6), 577–590.

Joussaume, S., Taylor, K.E., 1995. Status of the Paleoclimate Modeling Intercomparison Project (PMIP). In: Gates, W.L. (Ed.), Proceedings of the First International AMIP Scientific Conference. WCRP-92, WMO/TD-732, the World Meteorological Organization, Geneva, pp. 425–430. https://pmip1.lsce.ipsl.fr/publications/overview.html.

Jung, J.-H., Arakawa, A., 2004. The resolution dependence of model physics: illustrations from nonhydrostatic model experiments. J. Atmos. Sci. 61 (1), 88–102.

Jung, T., Gulev, S.K., Rudeva, I., Soloviov, V., 2006. Sensitivity of extratropical cyclone characteristics to horizontal resolution in the ECMWF model. Q. J. R. Meteorol. Soc. 132 (619), 1839–1857.

Kaufman, D., McKay, N., Routson, C., Erb, M., Dätwyler, C., Sommer, P.S., Oliver Heiri, O., Davis, B., 2020. Holocene global mean surface temperature, a multi-method reconstruction approach. Sci. Data 7, 201. https://doi.org/10.1038/s41597-020-0530-7.

Kageyama, M., Laîné, A., Abe-Ouchi, A., Braconnot, P., Cortijo, E., Crucifix, M., de Vernal, A., Guiot, J., Hewitt, C.D., Kitoh, A., Kucera, M., Marti, O., Ohgaito, R., Otto-Bliesner, B., Peltier, W.R., Rosell-Melé, A., Vettoretti, G., Weber, S.L., Yu, Y., MARGO Project members, 2006. Last Glacial Maximum temperatures over the North Atlantic, Europe and western Siberia: a comparison between PMIP models, MARGO sea-surface temperatures and pollen-based reconstructions. Quat. Sci. Rev. 25, 2082–2102.

Kageyama, M., Albani, S., Braconnot, P., Harrison, S.P., Hopcroft, P.O., Ivanovic, R.F., Lambert, F., Marti, O., Peltier, W.R., Peterschmitt, J.-Y., Roche, D.M., Tarasov, L., Zhang, X., Brady, E.C., Haywood, A.M., LeGrande, A.N., Lunt, D.J., Mahowald, N.M., Mikolajewicz, U., Nisancioglu, K.H., Otto-Bliesner, B.L., Renssen, H., Tomas, R.A., Zhang, Q., Abe-Ouchi, A., Bartlein, P.J., Cao, J., Li, Q., Lohmann, G., Ohgaito, R., Shi, X., Volodin, E., Yoshida, K., Zhang, X., Zheng, W., 2017. The PMIP4 contribution to CMIP6 – part 4: scientific objectives and experimental design of the PMIP4-CMIP6 Last Glacial Maximum experiments and PMIP4 sensitivity experiments. Geosci. Model. Dev. 10, 4035–4055. https://doi.org/10.5194/gmd-10-4035-2017.

Kasahara, A., 1966. The dynamical influence of orography on the large-scale motion of the atmosphere. J. Atmos. Sci. 23 (3), 259–271.

Kasahara, A., Sasamori, T., Washington, W.M., 1973. Simulation experiments with a 12-layer stratospheric global circulation model. I. Dynamical effect of the Earth's orography and thermal influence of continentality. J. Atmos. Sci. 30 (7), 1229–1251.

Kiehl, J.T., Williamson, D.L., 1991. Dependence of cloud amount on horizontal resolution in the national center for atmospheric research community climate model. J. Geophys. Res. 96 (D6), 10955–10980.

Kim, S.-J., Crowley, T.J., Erickson, D.J., Govindasamy, B., Duffy, P.B., Lee, B.Y., 2008. High-resolution climate simulation of the last glacial maximum. Clim. Dyn. 31, 1–16.

Knutti, R., Sedláček, J., 2012. Robustness and uncertainties in the new CMIP5 climate model projections. Nat. Clim. Change 3, 369–373. https://doi.org/10.1038/nclimate1716.

Kristjánsson, J.E., 1991. Cloud parametrization at different horizontal resolutions. Q. J. R. Meteorol. Soc. 117 (502), 1255–1280.

Kushnir, Y., Robinson, W.A., Bladé, I., Hall, N.M.J., Peng, S., Sutton, R., 2002. Atmospheric GCM response to extratropical SST anomalies: synthesis and evaluation. J. Clim. 15 (16), 2233–2256.

Laepple, T., Huybers, P., 2014. Ocean surface temperature variability: large model-data differences at decadal and longer periods. Proc. Natl. Acad. Sci. 111 (47), 16682–16687.

Lane, D.E., Somerville, R.C.J., Iacobellis, S.F., 2000. Sensitivity of cloud and radiation parameterizations to changes in vertical resolution. J. Clim. 13 (5), 915–922.

Lauer, A., Hamilton, K., 2013. Simulating clouds with global climate models: a comparison of CMIP5 results with CMIP3 and satellite data. J. Clim. 26 (11), 3823–3845.

Legutke, S., Voss, R., 1999. The Hamburg Atmosphere-Ocean Coupled Circulation Model ECHO-G. Deutsches Klimarechenzentrum, Hamburg, Germany, 18.

Lohmann, G., 2017. Atmospheric bridge on orbital time scales. Theor. Appl. Climatol. 128 (3), 709–718. https://doi.org/10.1007/s00704-015-1725-2.

Lohmann, G., Pfeiffer, M., Laepple, T., Leduc, G., Kim, J.H., 2013. A model and data comparison of the Holocene global sea surface temperature evolution. Clim. Past 9 (4), 1807–1839.

Lohmann, G., Butzin, M., Eissner, N., Shi, X., Stepanek, C., 2020. Abrupt climate and weather changes across timescales. Paleoceanogr. Paleoclimatol. 35 (9), e2019PA003782 https://doi.org/10.1029/2019PA003782.

Lorenz, S.J., Lohmann, G., 2004. Acceleration technique for Milankovitch type forcing in a coupled atmosphere-ocean circulation model: method and application for the Holocene. Clim. Dyn. 23 (7–8), 727–743.

Lutsko, N.J., Baldwin, J.W., Cronin, T.W., 2019. The impact of large-scale orography on Northern Hemisphere winter synoptic temperature variability. J. Clim. 32 (18), 5799–5814.

MacDonald, G.M., Velichko, A.A., Kremenetski, C.V., Borisova, O.K., Goleva, A.A., Andreev, A.A., Cwynar, L.C., Riding, R.T., Forman, S.L., Edwards, T.W.D., Aravena, R., Hammarlund, D., Szeicz, J.M., Gattaulin, V.N., 2000. Holocene treeline history and climate change across Northern Eurasia. Quat. Res. 53 (3), 302–311.

Manabe, S., Terpstra, T.B., 1974. The effects of mountains on the general circulation of the atmosphere as identified by numerical experiments. J. Atmos. Sci. 31 (1), 3–42.

Manabe, S., Smagorinsky, J., Holloway, J.L., Stone, H.M., 1970. Simulated climatology of a general circulation model with a hydrologic cycle. Mon. Weather. Rev. 98 (3), 175–212.

Mann, M., Rahmstorf, S., Kornhuber, K., Steinman, B.A., Miller, S.K., Coumou, D., 2017. Influence of anthropogenic climate change on planetary wave resonance and extreme weather events. Sci. Rep. 7, 45242.

Masato, G., Hoskins, B.J., Woollings, T., 2013. Winter and summer northern hemisphere blocking in CMIP5 models. J. Clim. 26 (18), 7044–7059.

Matsueda, M., Mizuta, R., Kusunoki, S., 2009. Future change in wintertime atmospheric blocking simulated using a 20-km-mesh atmospheric global circulation model. J. Geophys. Res. Atmos. 114, D12114 https://doi.org/10.1029/2009JD011919.

Monnin, E., Indermühle, A., Dällenbach, A., Flückiger, J., Stauffer, B., Stocker, T.F., Raynaud, D., Barnola, J.-M., 2001. Atmospheric CO2 concentrations over the last glacial termination. Science 291 (5501), 112–114.

Nam, C.C.W., Quaas, J., 2012. Evaluation of clouds and precipitation in the ECHAM5 general circulation model using CALIPSO and CloudSat satellite data. J. Clim. 25 (14), 4975–4992.

Otto-Bliesner, B., Schneider, R., Brady, E., Kucera, M., Abe-Ouchi, A., Bard, E., Braconnot, P., Crucifix, M., Hewitt, C., Kageyama, M., Marti, O., Paul, A., Rosell-Melé, A., Waelbroeck, C., Weber, S., Weinelt, M., Yu, Y., 2009. A comparison of PMIP2 model simulations and the MARGO proxy reconstruction for tropical sea surface temperatures at last glacial maximum. Clim. Dyn. 32 (6), 799–815.

Otto-Bliesner, B.L., Braconnot, P., Harrison, S.P., Lunt, D.J., Abe-Ouchi, A., Albani, S., Bartlein, P.J., Capron, E., Carlson, A.E., Dutton, A., Fischer, H., Goelzer, H., Govin, A., Haywood, A., Joos, F., LeGrande, A.N., Lipscomb, W.H., Lohmann, G., Mahowald, N., Nehrbass-Ahles, C., Pausata, F.S.R., Peterschmitt, J.-Y., Phipps, S. J., Renssen, H., Zhang, Q., 2017. The PMIP4 contribution to CMIP6 – part 2: two interglacials, scientific objective and experimental design for Holocene and Last Interglacial simulations. Geosci. Model. Dev. 10, 3979–4003.

Pfeiffer, M., Lohmann, G., 2016. Greenland Ice Sheet influence on Last Interglacial climate: global sensitivity studies performed with an atmosphere?ocean general circulation model. Clim. Past 12, 1313–1338. https://doi.org/10.5194/cp-12-1313-2016.

Petoukhov, V., Rahmstorf, S., Petri, S., Schellnhuber, H.J., 2013. Quasiresonant amplification of planetary waves and recent Northern Hemisphere weather extremes. Proc. Natl. Acad. Sci. 110, 5336–5341.

Pope, Stratton, 2002. The processes governing horizontal resolution sensitivity in a climate model. Clim. Dyn. 19 (3), 211–236.

Potter, G.L., 1995. The Effect of Horizontal Resolution on Cloud Radiative Forcing in the ECMWF Model. Lawrence Livermore National Laboratory, Livermore, CA, USA. PCMDI Report No. 22.

Prentice, C., Guiot, J., Huntley, B., Jolly, D., Cheddadi, R., 1996. Reconstructing biomes from palaeoecological data: a general method and its application to European pollen data at 0 and 6 ka. Clim. Dyn. 12 (3), 185–194.

Randall, D.A., Wood, R.A., Bony, S., Colman, R., Fichefet, T., Fyfe, J., Kattsov, V., Pitman, A., Shukla, J., Srinivasan, J., Stouffer, R.J., Sumi, A., KE, T., 2007. Climate models and their evaluation. In: Solomon, S., Qin, D., Manning, M., Chen, Z., Marquis, M., Averyt, K.B., Tignor, M., Miller, H.L. (Eds.), Chapter 8 in Climate Change 2007: the Physical Science Basis. Contribution of Working Group I to the Fourth Assessment Report of the Intergovernmental Panel on Climate Change. Cambridge University Press, Cambridge, UK.

Reichler, T., Kim, J., 2008. How well do coupled models simulate today's climate? Bull. Am. Meteorol. Soc. 89 (3), 303–311.

Rimbu, N., Lohmann, G., Ionita, M., 2014. Interannual to multidecadal Euro-Atlantic blocking variability during winter and its relationship with extreme low temperatures in Europe. J. Geophys. Res. Atmos. 119 (24), 13621–13636.

Rind, D., 1988. Dependence of warm and cold climate depiction on climate model resolution. J. Clim. 1 (10), 965–997.

Roeckner, E., Bäuml, G., Bonaventura, L., Brokopf, R., Esch, M., Giorgetta, M., Hagemann, S., Kirchner, I., Kornblueh, L., Manzini, E., Rhodin, A., Schlese, U., Schulzweida, U., Tompkins, A., 2003. The atmospheric general circulation model ECHAM5. Part I. Max-Planck-Institut für Meteorologie Reports. No. 349.

Roeckner, E., Brokopf, R., Esch, M., Giorgetta, M., Hagemann, S., Kornblueh, L., Manzini, E., Schlese, U., Schulzweida, U., 2006. Sensitivity of simulated climate to horizontal and vertical resolution in the ECHAM5 atmosphere model. J. Clim. 19 (16), 3771–3791.

Scaife, A.A., Woollings, T., Knight, J., Martin, G., Hinton, T., 2010. Atmospheric blocking and mean biases in climate models. J. Clim. 23 (23), 6143–6152.

Schulzweida, U., Kornblueh, L., Quast, R., 2009. CDO—Climate Data Operators-Project Management Service (Version 1.4.1). Max Planck Institute for Meteorology, Hamburg, Germany. https://code.zmaw.de/projects/cdo.

Seppä, H., Birks, H.J.B., 2001. July mean temperature and annual precipitation trends during the Holocene in the Fennoscandian tree-line area: pollen-based climate reconstructions. Holocene 11 (5), 527–539.
Shi, X., Lohmann, G., 2016. Simulated response of the mid-holocene atlantic meridional overturning circulation in ECHAM6-FESOM/MPIOM. J. Geophys. Res. Oceans 121 (8), 6444–6469.
Shi, X., Lohmann, G., Sidorenko, D., Yang, H., 2020. Early-holocene simulations using different forcings and resolutions in AWI-ESM. Holocene 30 (7), 996–1015.
Simmonds, I., Smith, I.N., 1986. The effect of the prescription of zonally-uniform sea surface temperatures in a general circulation model. J. Climatol. 6 (6), 641–659.
Sundqvist, H.S., Zhang, Q., Moberg, A., Holmgren, K., Körnich, H., Nilsson, J., Brattström, G., 2010. Climate change between the mid and late Holocene in northern high latitudes – part 1: survey of temperature and precipitation proxy data. Clim. Past 6 (5), 591–608.
Tarasov, P.E., Webb, T., Andreev, A.A., Natalya, B.A.E., Berezina, N.A., Bezusko, L.G., Blyakharchuk, T.A., Bolikhovskaya, N.S., Cheddadi, R., Chernavskaya, M.M., Chernova, G.M., Dorofeyuk, N.I., Dirksen, V.G., Elina, G.A., Filimonova, L.V., Glebov, F.Z., Guiot, J., Gunova, V.S., Harrison, S.P., Jolly, D., Khomutova, V.I., Kvavadze, E.V., Osipova, I.M., Panova, N.K., Prentice, I.C., Saarse, L., Sevastyanov, D.V., Volkova, V.S., Zernitskaya, V.P., 1998. Present-day and mid-holocene biomes reconstructed from pollen and plant macrofossil data from the Former Soviet Union and Mongolia. J. Biogeogr. 25 (6), 1029–1053.
Taylor, K.C., Williamson, D., Zwiers, F.W., 2000. The sea surface temperature and sea-ice concentration boundary conditions for AMIP II simulations. PCMDI Report No. 60, Program for Climate Model Diagnosis and Intercomparison. University of California, Lawrence Livermore National Laboratory, Livermore, CA 94550.
Tibaldi, S., Palmer, T.N., Brankovic, C., Cubasch, U., 1990. Extended-range predictions with ECMWF models: influence of horizontal resolution on systematic error and forecast skill. Q. J. R. Meteorol. Soc. 116, 835–866.
Tselioudis, G., Jakob, C., 2002. Evaluation of midlatitude cloud properties in a weather and a climate model: dependence on dynamic regime and spatial resolution. J. Geophys. Res. 107 (D24), 4781.
Varma, V., Prange, M., Merkel, U., Kleinen, T., Lohmann, G., Pfeiffer, M., Renssen, H., Wagner, A., Wagner, S., Schulz, M., 2012. Holocene evolution of the Southern Hemisphere westerly winds in transient simulations with global climate models. Clim. Past 8, 391–402. https://doi.org/10.5194/cp-8-391-2012.
Varma, V., Prange, M., Schulz, M., 2016. Transient simulations for present and last interglacials using a comprehensive coupled climate model CCSM3 (Community Climate System Model 3.0), links to model result files in NetCDF format. Geosci. Model. Dev. 9 (11), 3859–3873.
Vavrus, S., Philippon-Berthier, G., Kutzbach, J.E., Ruddiman, W.F., 2011. The role of GCM resolution in simulating glacial inception. Holocene 21 (5), 831–842.
Viau, A.E., Gajewski, K., Sawada, M.C., Fines, P., 2006. Millennial-scale temperature variations in North America during the Holocene. J. Geophys. Res. Atmos. 111, D09102 https://doi.org/10.1029/2005JD006031.
Wei, W., Lohmann, G., 2012. Simulated atlantic multidecadal oscillation during the holocene. J. Clim. 25, 6989–7002. https://doi.org/10.1175/JCLI-D-11-00667.1.
Werner, M., Jouzel, J., Masson-Delmotte, V., Lohmann, G., 2018. Reconciling glacial-interglacial changes of Antarctic water stable isotopes, ice sheet topography, and the isotopic paleothermometer. Nat. Commun. 9, 3537. https://doi.org/10.1038/s41467-018-05430-y.
Williamson, D.L., Kiehl, J.T., Hack, J.J., 1995. Climate sensitivity of the NCAR Community Climate Model (CCM2) to horizontal resolution. Clim. Dyn. 11 (7), 377–397.
Wills, R.C.J., White, R.H., Levine, X.J., 2019. Northern hemisphere stationary waves in a changing climate. Curr. Clim. Change Rep. 5, 372–389.
Yoshino, M.M., 1981. Orographically-induced atmospheric circulations. Prog. Phys. Geogr. 5 (1), 76–98.
Zhang, X., Lohmann, G., Knorr, G., Xu, X., 2013. Different ocean states and transient characteristics in Last Glacial Maximum simulations and implications for deglaciation. Clim. Past 9, 2319–2333. https://doi.org/10.5194/cp-9-2319-2013.
Zhang, X., Lohmann, G., Knorr, G., Purcell, C., 2014. Abrupt glacial climate shifts controlled by ice sheet changes. Nature 512, 290–294. https://doi.org/10.1038/nature13592.
Zheng, W., Braconnot, P., Guilyardi, E., Merkel, U., Yu, Y., 2008. ENSO at 6ka and 21ka from ocean–atmosphere coupled model simulations. Clim. Dyn. 30 (7), 745–762.